Atmospheric
Chemistry
and Physics

Open Access

EGU

Supplement of

Shipborne measurements of ClNO$_2$ in the Mediterranean Sea and around the Arabian Peninsula during summer

Philipp G. Eger et al.

*Correspondence to:* John N. Crowley (john.crowley@mpic.de)
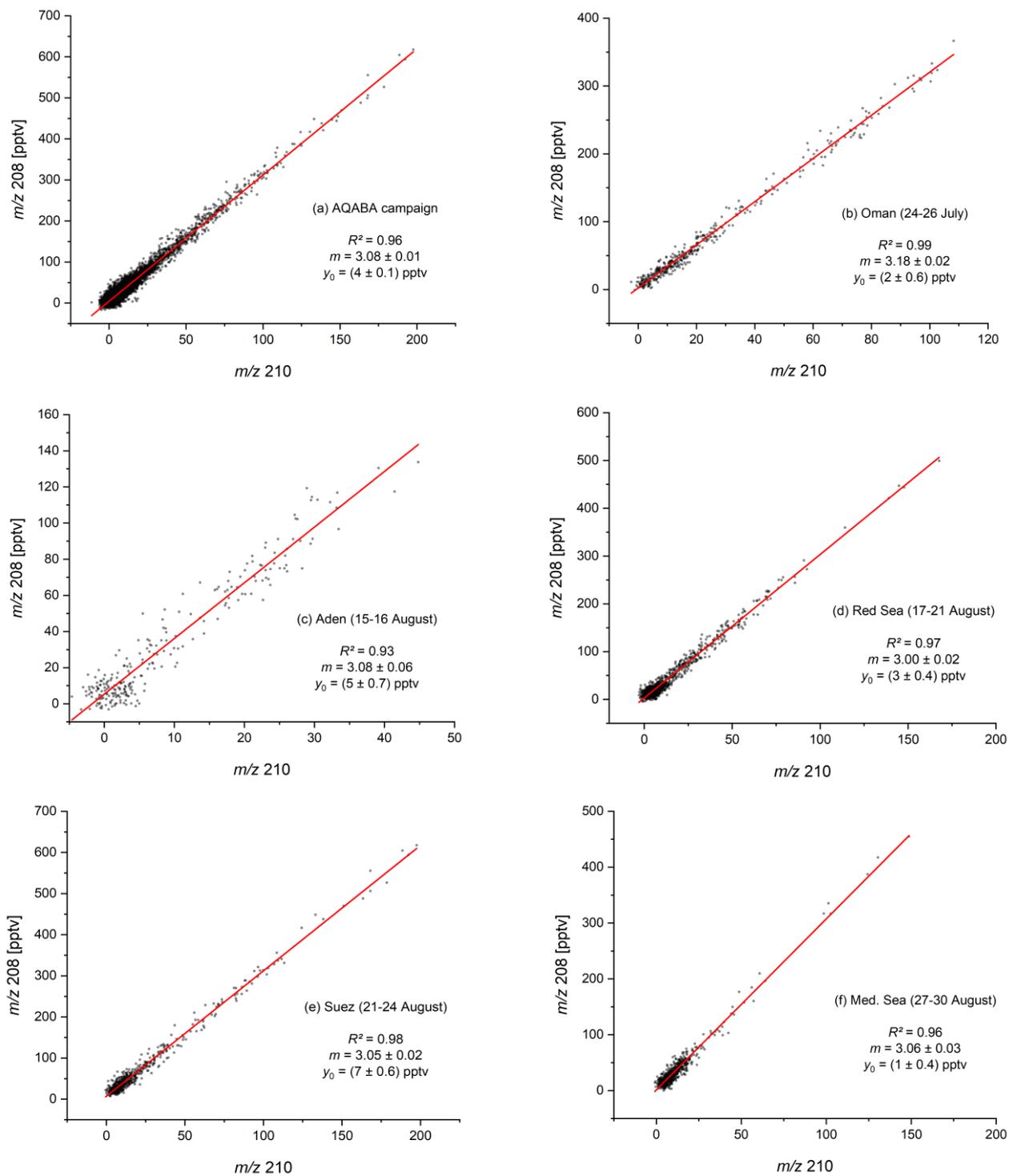
Figure S1: Correlation between relative ClNO$_2$ signals measured at *m/z* 208 and 210 (with slope *m* and intercept y_0) for (a) the AQABA campaign and (b–f) selected periods in the Gulf of Oman, the Gulf of Aden, the Red Sea, the Suez Canal and the Mediterranean Sea.

Corrections to the aerosol particle surface area concentration

To derive the ambient PM_1 particle surface area concentration A from the measured dry particle surface area concentration (AMS) we applied a hygroscopic growth factor based on ambient RH and PM_1 aerosol composition. From the AMS measurements we derived the molar ratio of sulphate to ammonium of ≈ 2.2 (see Fig. S2), which is close to the ratio of ≈ 2 for completely neutralised ammonium-sulphate aerosol, indicating its dominance in the fine mode during AQABA. For most of the campaign $(NH_4^+)_2(SO_4^{2-})$ contributed 80-100 % to the total inorganic PM_1 aerosol mass (see Fig. S3) while nitrate and chloride were less abundant. A relative humidity-dependent growth factor G_{amsu} for the particle diameter was calculated using the parameterisation (Eq. S1) of Lewis (2008) for pure ammonium-sulphate drops with a = 0.78 and b = 1.90.

$$G_{amsu}(RH) = a \left(b + \frac{1}{1-RH} \right)^{1/3} \tag{S1}$$

The growth factor was calculated considering the RH of the sample air after passing the aerosol dryer (see Sect. 2.5 in the manuscript) which was usually in the range 40 ± 10 %. To account for the organic mass fraction we calculated the volume fraction v_{org} of organics using a typical density of 1400 kg/m³ for oxidised organics in aged atmospheric aerosol (Gysel et al., 2007) and the volume fraction v_{amsu} of $(NH_4^+)_2(SO_4^{2-})$, assuming that all NH_4^+ and SO_4^{2-} measured originated from ammonium-sulphate. In the next step we derived a combined growth factor by applying a mixing rule (Eq. S2) where the water activity a_w was approximated by the relative humidity (Gysel et al., 2007):

$$G_{mixed} \approx \left(\sum_i v_i \, G_i^3 \right)^{\frac{1}{3}} \tag{S2}$$

For the organic fraction a growth factor of $G_{org} = 1.20 \pm 0.10$ at $a_w = 0.9$ and a ratio of $\frac{G_{org}}{G_{amsu}} \approx \frac{1.20}{1.80}$ was reported by Gysel et al. (2007). Assuming a similar RH-dependence for G_{org} than for G_{amsu} results in Eq. S3 which can be inserted into Eq. S2 along with Eq. S1.

$$G_{org} \approx 1 + \frac{1}{4}(G_{amsu} - 1) \tag{S3}$$

The resulting surface area growth factor $G_A = (G_{mixed})^2$ as a function of RH is shown in Fig. S4. The particle surface area concentration (PM_1) reported in Table 1 of the manuscript already includes this correction. The distribution of surface area growth factors for the whole AQABA campaign is shown in Fig. S5 and has a campaign average of 1.32 ± 0.24.
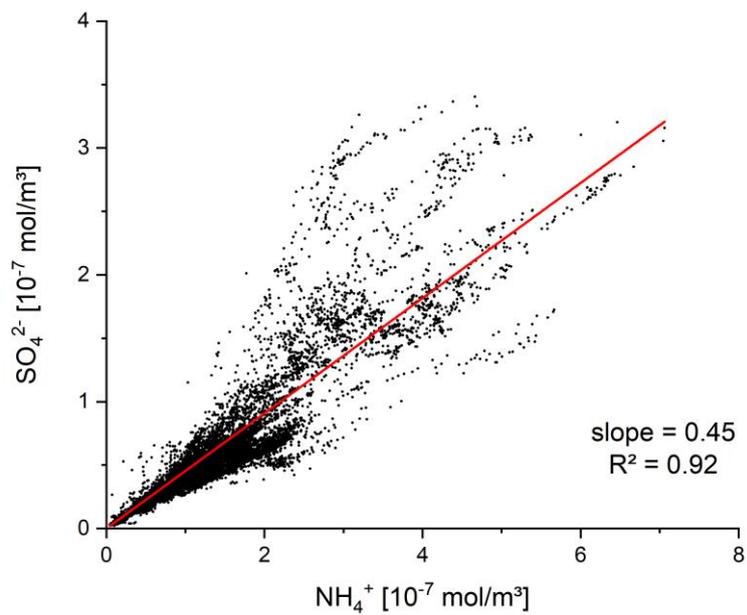
Figure S2: Correlation between PM_1 (AMS) ammonium and sulphate (in mol m^{-3}).
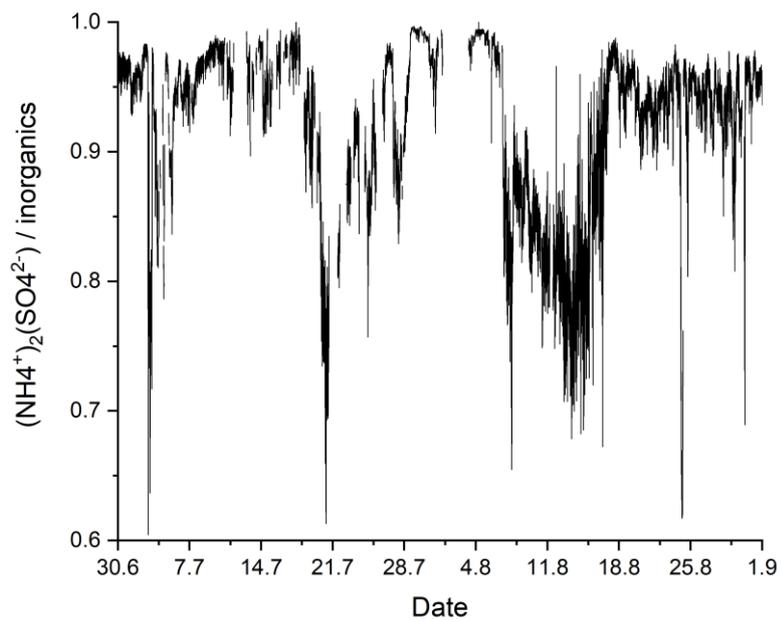

Figure S3: Contribution of ammonium-sulphate to the total non-refractory inorganic PM_1 aerosol mass.
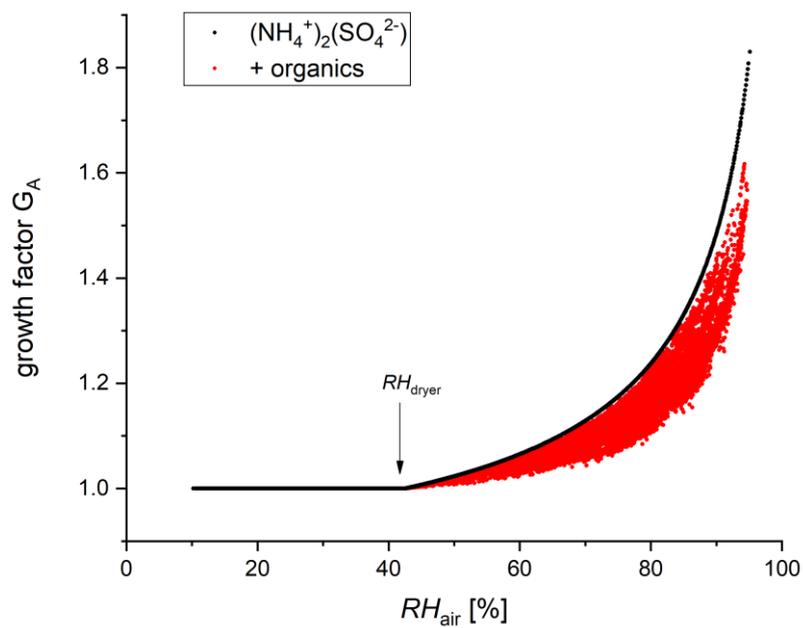
Figure S4: Surface growth factors for pure ammonium-sulphate (black) and for a mixture with organics (red).
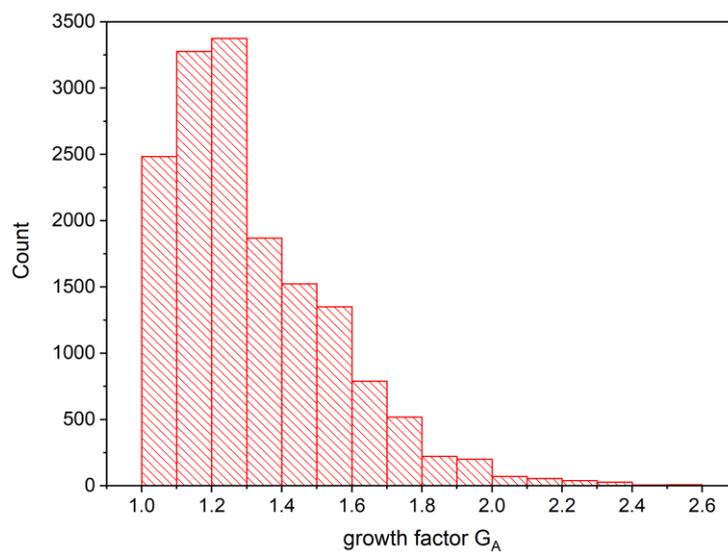

Figure S5: Distribution of calculated surface area growth factors G_A for the whole AQABA campaign.

5
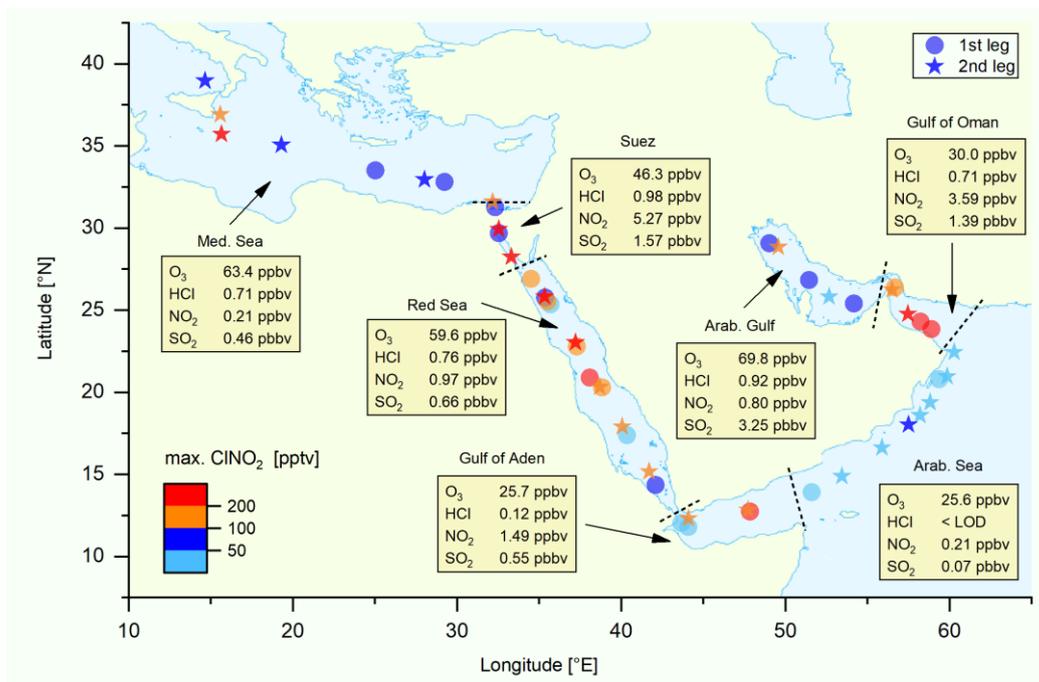
**Figure S6**: Map of maximum ClNO$_2$ mixing ratios on individual nights together with (median) night-time mixing ratios of O$_3$, HCl, NO$_2$ and SO$_2$ for different regions demarked by dashed lines. Circles and stars represent data obtained on the first and second legs, respectively.
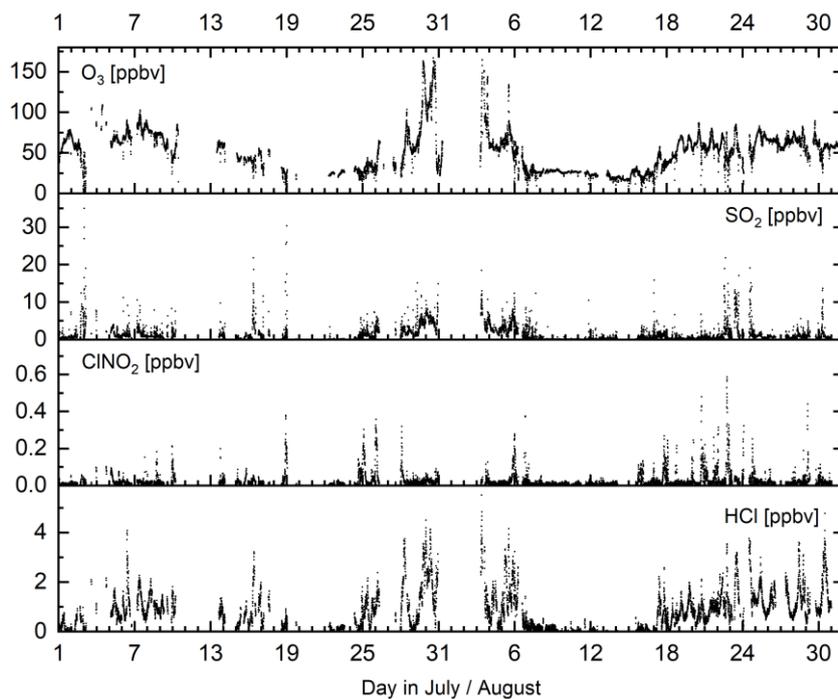
Figure S7: Time series of O$_3$, SO$_2$, ClNO$_2$ and HCl mixing ratios during the AQABA campaign.
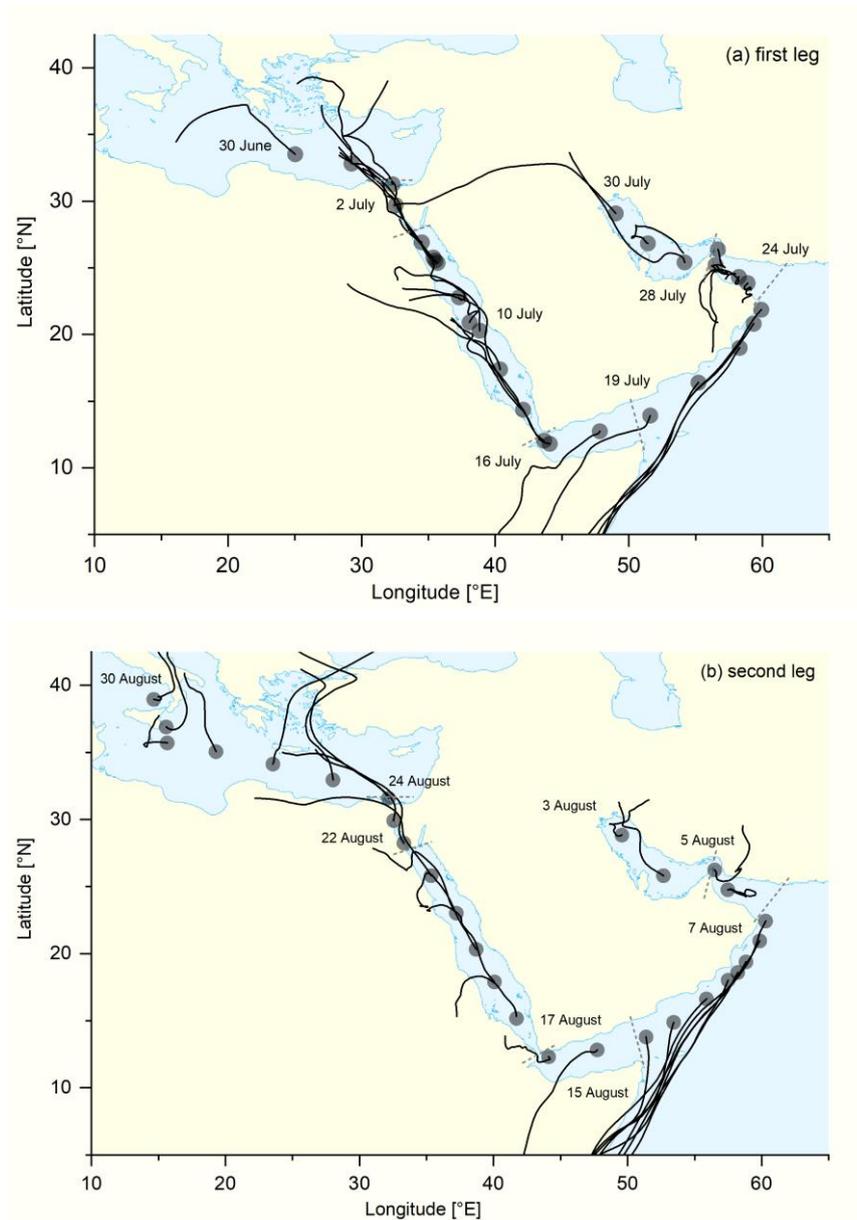
5

Figure S8: 48-h back-trajectories calculated with HYSPLIT (at 100 m above sea-level) representative for the corresponding nights.
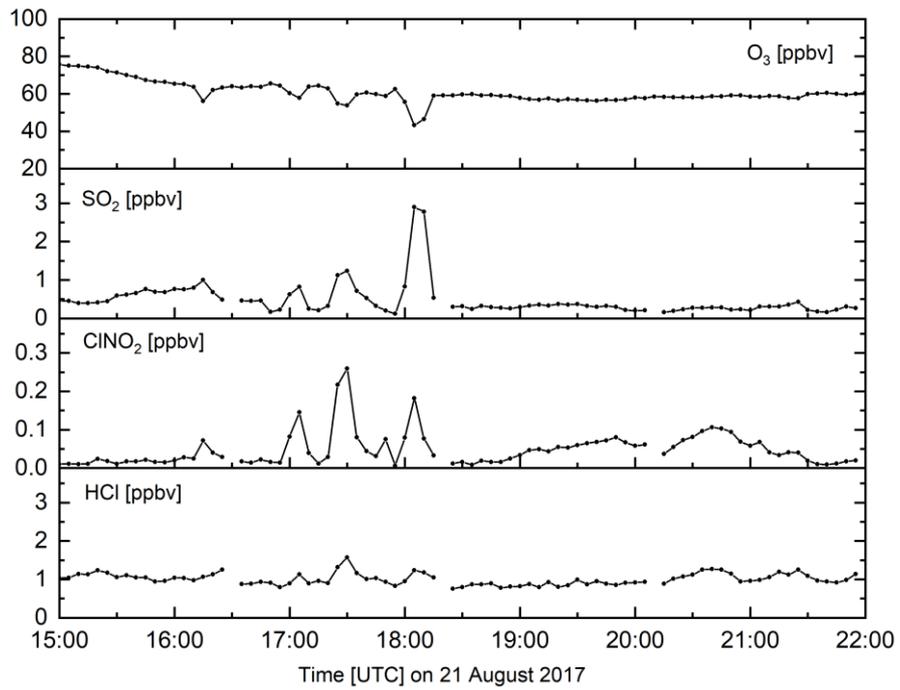
Figure S9: Observation of $ClNO_2$ in distinct ship plumes between 16:30 and 18:30 UTC (indicated by increased SO_2 mixing ratios and O_3 titration due to NO) on 21 August 2017 in the Red Sea.
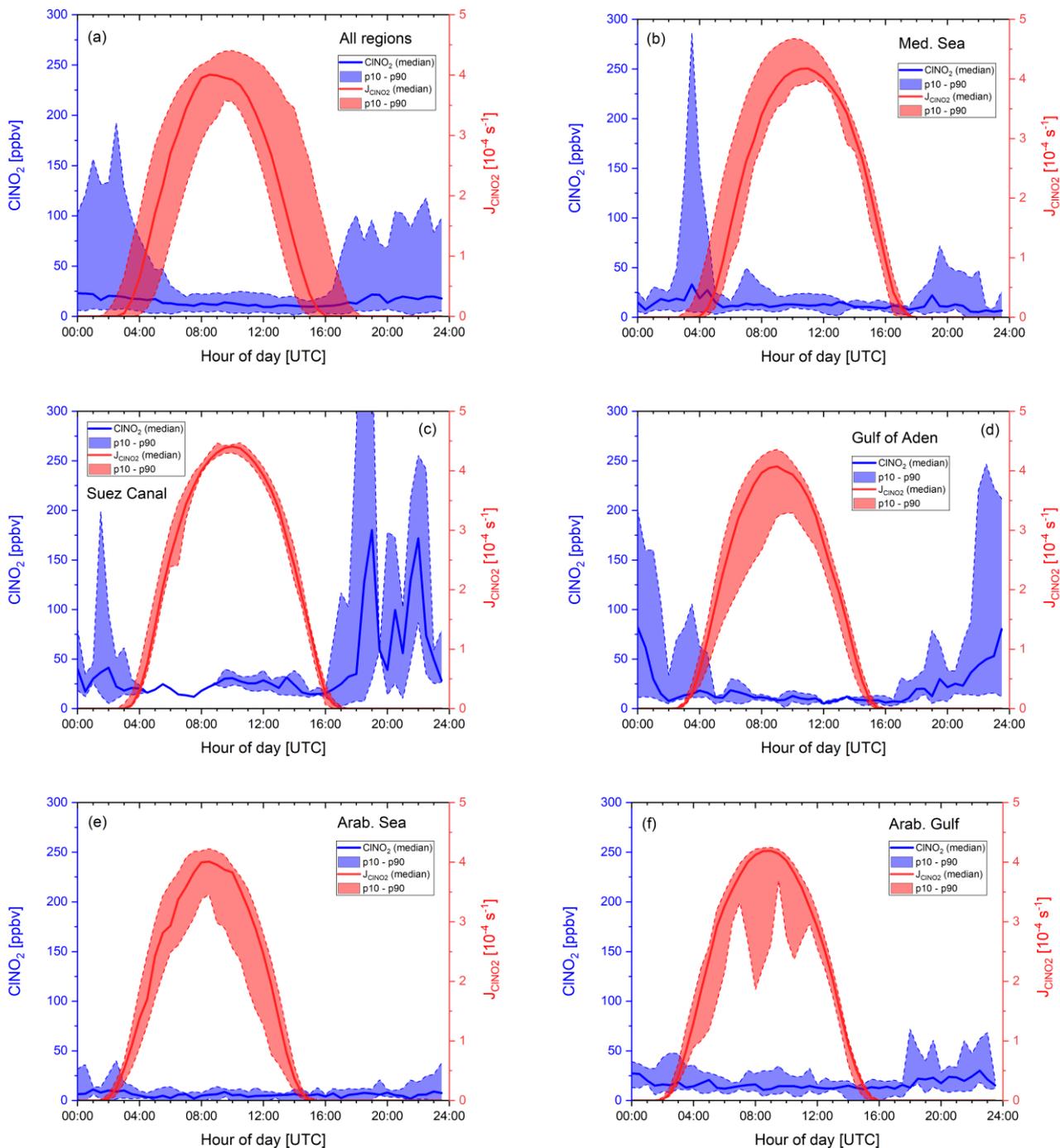
Figure S10: Diurnal profiles of ClNO2 for (a) all regions combined, (b) the Mediterranean Sea, (c) the Suez Canal and Gulf of Suez, (d) the Gulf of Aden, (e) the Arabian Sea, and (f) the Arabian Gulf. p10 and p90 correspond to the 10th and 90th percentiles.

Additional details to the derivation of the ClNO₂ production efficiency ε

To investigate the uncertainty related to assumptions made in the calculation of ε, we define five different methods A–E and

5   compare them to each other by applying them to the whole AQABA dataset (Fig. S11).

Method A: The starting point t_0 for NO_3 formation is set to sunset minus 40 ± 10 min as described in the manuscript but all data points before sunset were excluded from the analysis due to a large uncertainty in reaction time. This way $N_A = 4175$ values of ε were obtained throughout the campaign. In *Method A*, we inherently assume that the air mass we probe has not been influenced by fresh NO emissions since the beginning of the night. A fresh NO emission would mean that the air mass

10   at the beginning of the night would have contained less NO_2 than calculated in Eq. 3 resulting in an overestimation of the integrated NO_3 production and thus values of ε calculated by *Method A* represent a lower limit.

Method B: To account for fresh emissions of NO (e.g. by passing ships), the reaction time *t'* was calculated from Eq. 5 where *s* represents the number of NO_2 molecules required to make NO_y and is 1 when NO_3 reacts directly with VOCs and 2 when NO_3 reacts with NO_2 to form N_2O_5, which subsequently hydrolyses to HNO_3. As discussed later, the direct NO_3 losses are

15   dominant throughout the campaign compared to the heterogeneous N_2O_5 production, so to a good approximation, $s = 1$. As discussed by McDuffie et al. (2018) inherent to the use of this expression is the assumption that NO_y is conserved during the night; any losses of NO_y (e.g. via deposition of HNO_3) leading to an underestimation of the true reaction time. Whenever *t'* is shorter than the time elapsed since sunset (see *Method A*), *t'* is used to integrate the NO_3 production term. As the calculated, night-time air mass age depends on the ratio between $[NO_2]$ and $[NO_y]$, the calculation breaks down whenever a fresh NO

20   emission (e.g. from a nearby ship) is injected into an air-mass and unreacted NO is still present. In this case the NO_2 to NO_y ratio would be decreased and the age of the air-mass overestimated. To avoid this, we only use data where NO is below the detection limit, resulting in a total number of $N_B = 2987$ data points.

Method C: Here we only consider data points where the calculated age of the air mass (as derived in *Method B*) is equal to or exceeds the time elapsed since sunset as derived in *Method A*. These air masses are unlikely to have been impacted by recent

25   emission. As loss of NO_z by deposition will result in an air mass age that is shorter than the true one, we relax the criterion for equality of reaction times by also including calculated air mass ages that are up to 25 % shorter (i.e. $t' \geq 0.75\,(t - t_0)$). The resulting dataset is reduced to $N_C = 1742$ data points. All values of ε discussed in the manuscript were derived using method C.

Method D: ClNO₂ mixing ratios close to the limit of detection (LOD) result in a higher uncertainty and variability in ε,

30   especially when the NO_3 production term is also small. In *Method D*, we use only data in which the ClNO₂ mixing ratio is at least 25 pptv, which represents the LOD + the median, daytime HCl-interference (Sect. 3.1). This drastically reduces the size of the dataset to $N_D = 280$ data points.

Method E: In method E, we examine the efficiency of ClNO$_2$ formation only during a few nights when its mixing ratio exceeded 100 pptv. The intention here is not to derive e.g. a regional mean value, but to indicate that even when biasing the dataset to apparently efficient ClNO$_2$ generation, ε remains low. In *Method E*, only $N_E = 50$ data points remain (1.2% of the dataset analysed in *Method A*).

We summarise values of ε as median and mean values for the entire campaign in Fig. S11, segregated into the five different methods used to select data and derive the reaction time. As described earlier, *Method A* can be understood as a lower limit for ε providing a median efficiency of only 1.4 % with a range from 0–8 % (10th and 90th percentiles) and a large difference between mean and median values. More reliable median values of ε = 2.8 % and 2.7 % are provided by *Methods B and C*. *Method D*, results in identical median and mean values of ε = 4.5 %, although a bias towards higher values is difficult to rule out as low ClNO$_2$ mixing ratios were excluded. For *Method E*, where we only consider data with ClNO$_2$ > 100 pptv, we derive a larger median value of ε = 6.4 %. If we consider only the individual maxima in the ClNO$_2$ mixing ratio (above 100 pptv) on any particular night, we derive 17 values of ε that vary between 1.1 and 11.2 % which are listed in Table S1.

In our manuscript (Fig. 5 and 6) we exclusively report values of ε derived by *Method C*. In comparison to Fig. 6 in the manuscript, Figure S12 illustrates how the box-plots for the seven regions would be altered when applying *Method D* instead of *Method C*. The variability is generally decreased and median values are shifted towards higher values, but the general picture and conclusions are not changed.
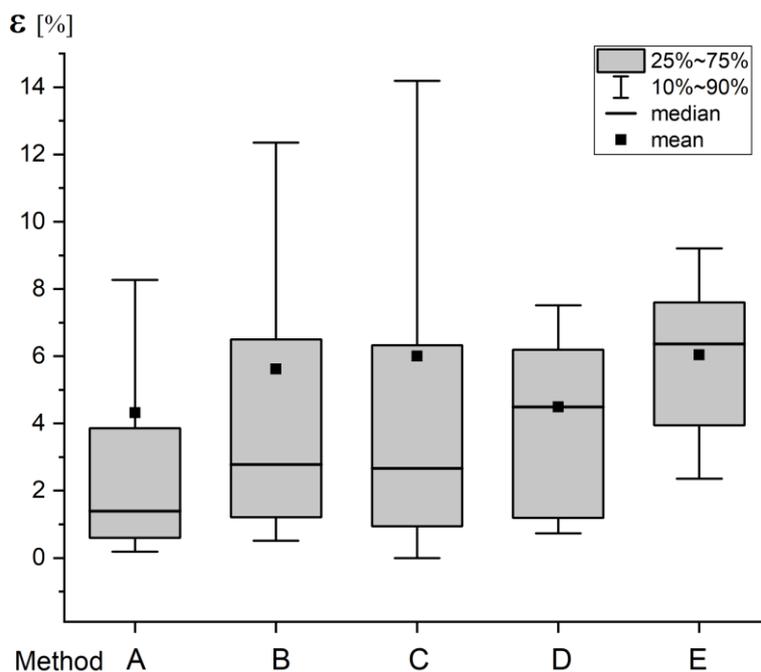

Figure S11: Box plot of ε derived by the different methods A–E for the whole AQABA campaign. The whiskers represent the 10th and 90th percentiles.
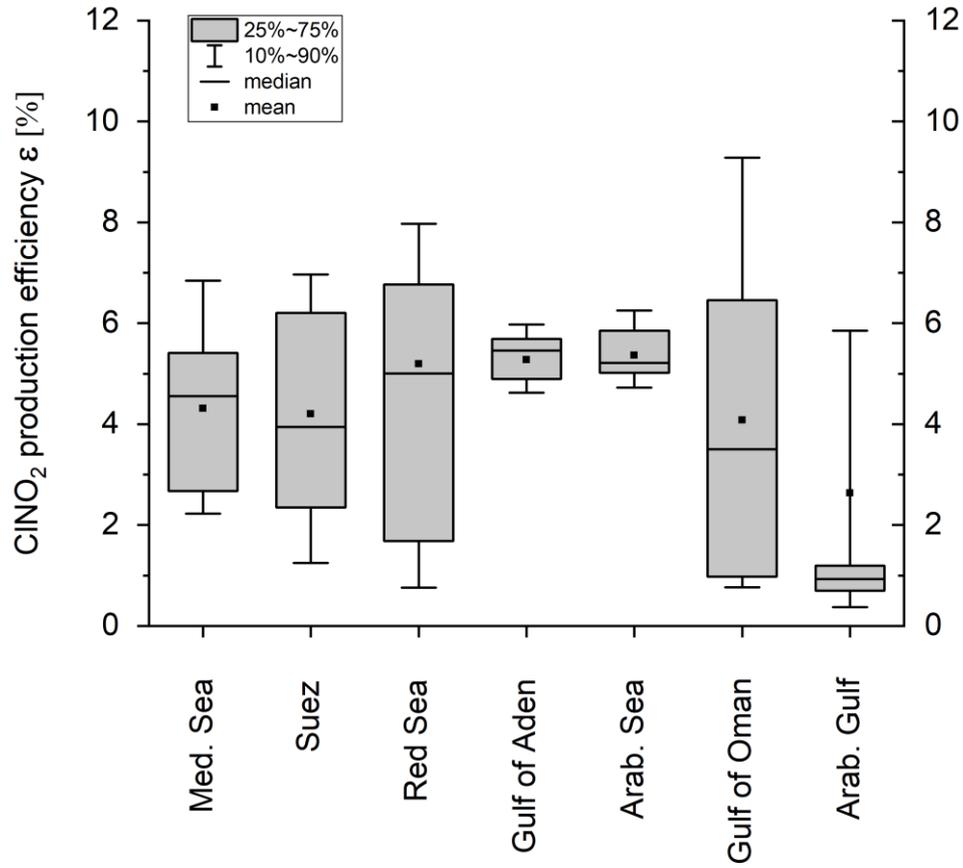
Figure S12: Median values of ε (ClNO$_2$ production efficiency) for each region, calculated from individual night-time values (between 10 and 104 per region) based on Eq. 4 in the manuscript but using method D instead of method C.

5
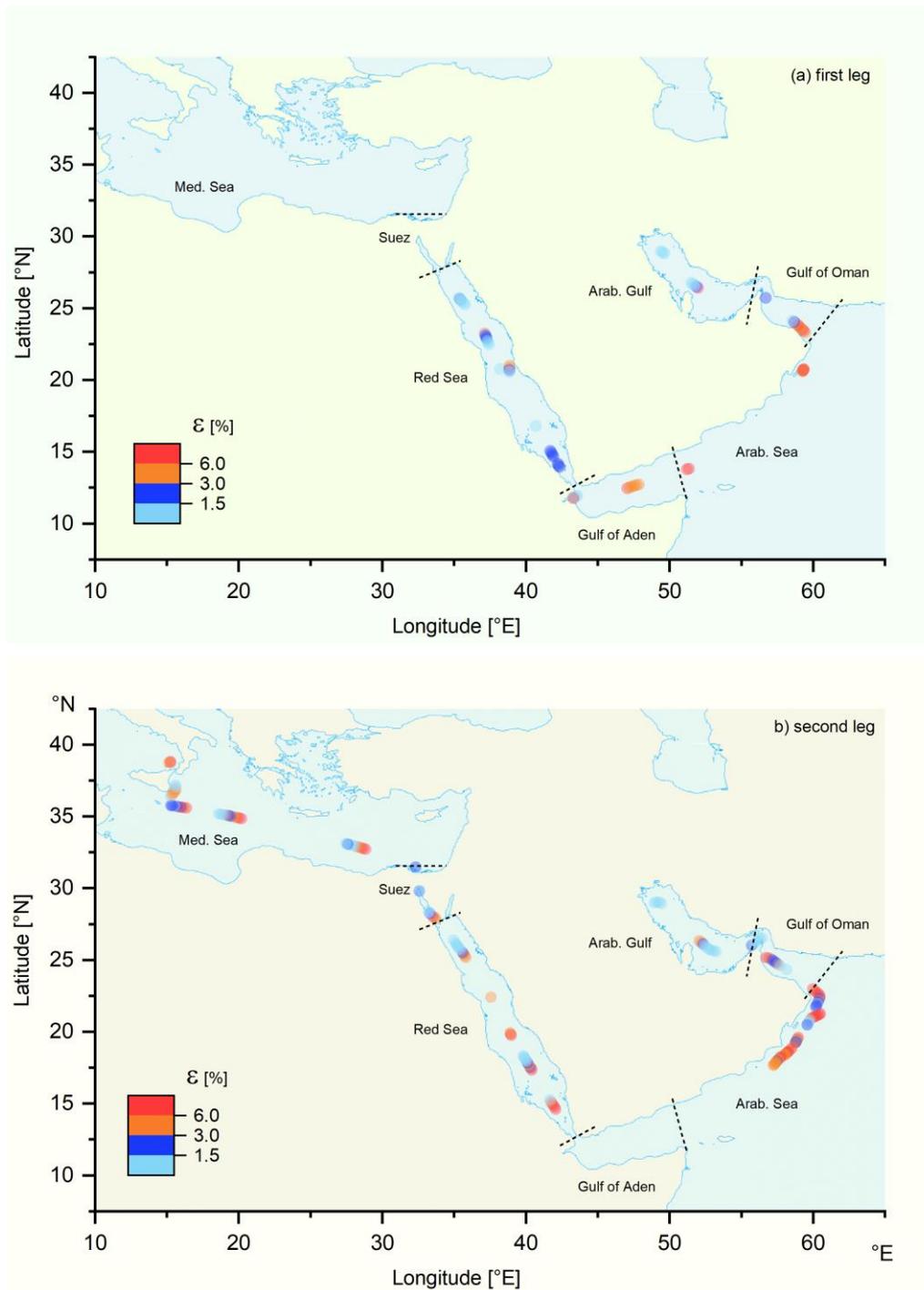
Figure S13: 1-hour averaged values of ε along the ship track for (a) first and (b) second leg, calculated via Eq. (4).

5
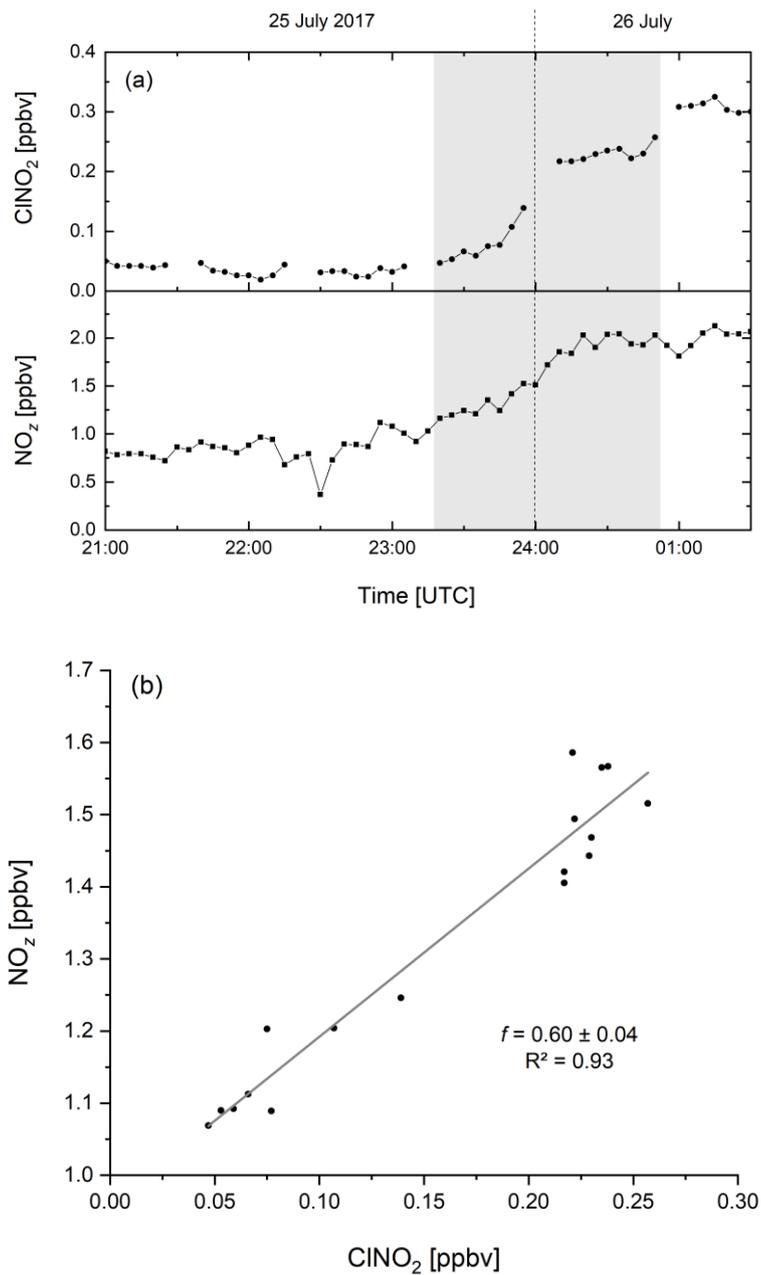
Figure S14: (a) Time series of ClNO2 and NO$_z$ on 25–26 July 2017 in the Gulf of Oman. (b) The slope of NO2 vs. ClNO2 can be used (Eq. 9) to calculate $f = 0.60 \pm 0.04$ for the ~ 2 h period (grey shaded area in Fig.S14a).

13

Table S1: Observed ClNO$_2$ plumes (typical duration of one to several hours) with mixing ratios above 100 pptv.

Date, time [UTC]	Region	t [h]	t' [h]	ClNO$_2$ [pptv]	N$_2$O$_5$ [pptv]	NO$_{3,\,int}$ [ppbv]	ε [%]	O$_3$ [ppbv]	SO$_2$ [ppbv]	HCl [ppbv]	NO$_2$ [ppbv]
08.07. 17:50	Red Sea	1.8	1.5	128	-	3.17	4.0	61.5	3.0	1.1	6.9
24.07. 16:05	Oman	1.8	2.3	143	-	1.28	1.1	25.7	1.1	0.3	7.0
03.08. 18:00	Arab. Gulf	2.9	2.6	115	53	9.65	1.2	78.8	3.0	1.8	6.7
06.08. 18:45	Oman	4.3	3.9	173	-	1.55	1.1	28.1	1.4	0.7	2.9
06.08. 20:35	Oman	6.1	6.9	159	-	2.86	5.6	20.0	4.0	0.6	5.2
17.08. 18:00	Red Sea	3.0	4.5	120	9	1.54	7.8	34.4	1.6	0.7	3.2
17.08. 19:25	Red Sea	4.4	3.6	212	14	3.03	7.0	34.7	2.1	1.8	3.9
17.08. 20:05	Red Sea	5.1	4.7	168	8	2.03	8.3	32.0	1.3	1.5	2.4
18.08. 17:00	Red Sea	1.8	1.5	106	23	1.49	7.1	42.9	0.9	0.6	4.6
20.08. 16:45	Red Sea	1.3	1.0	144	59	1.90	7.6	58.7	0.7	1.0	5.8
21.08. 17:05	Red Sea	1.5	1.4	145	53	2.13	6.8	57.9	0.8	1.1	5.9
21.08. 17:30	Red Sea	1.9	2.5	259	87	3.14	8.2	53.8	1.2	1.6	7.1
21.08. 23:40	Red Sea	8.1	8.5	103	27	9.78	1.1	58.0	0.7	1.1	2.3
22.08. 16:50	Suez	1.0	1.3	123	118	1.96	6.3	45.7	2.5	1.2	11.4
22.08. 18:20	Suez	2.5	2.1	586	355	7.09	8.3	56.4	4.6	3.5	11.3
22.08. 21:40	Suez	5.8	4.6	308	52	8.77	3.5	39.4	1.2	1.2	7.6
22.08. 22:30	Suez	6.7	6.1	222	47	9.45	2.3	43.0	1.0	1.1	5.9

[1] Notes: Red Sea, Gulf of Oman (Oman), Arabian Gulf (Arab. Gulf) and Suez Canal / Gulf of Suez (Suez). t denotes the time since sunset; t' corresponds to the air mass age calculated from Eq. 5 in the manuscript NO$_{3,int}$ is the total amount of NO$_3$ produced over the course of the night and ε is the ClNO$_2$ production efficiency (Eq. 4 in manuscript).

References

Gysel, M., Crosier, J., Topping, D., Whitehead, J., Bower, K., Cubison, M., Williams, P., Flynn, M., McFiggans, G., and
Coe, H.: Closure study between chemical composition and hygroscopic growth of aerosol particles during TORCH2, Atmos.
Chem. Phys., 7, 6131-6144, 2007.

Lewis, E. R.: An examination of Köhler theory resulting in an accurate expression for the equilibrium radius ratio of a
hygroscopic aerosol particle valid up to and including relative humidity 100%, Journal of Geophysical Research:
Atmospheres, 113, 2008.

McDuffie, E. E., Fibiger, D. L., Dubé, W. P., Lopez-Hilfiker, F., Lee, B. H., Thornton, J. A., Shah, V., Jaeglé, L., Guo, H.,
and Weber, R. J.: Heterogeneous N_2O_5 uptake during winter: Aircraft measurements during the 2015 WINTER campaign
and critical evaluation of current parameterizations, Journal of Geophysical Research: Atmospheres, 123, 4345-4372, 2018.